J Biomol NMR (2011) 49:99–109
DOI 10.1007/s10858-011-9470-z

ARTICLE

Extension of the HA-detection based approach: (HCA)CON(CA)H and (HCA)NCO(CA)H experiments for the main-chain assignment of intrinsically disordered proteins

Sampo Mäntylahti · Maarit Hellman · Perttu Permi

Received: 29 September 2010 / Accepted: 22 December 2010 / Published online: 25 January 2011

Abstract Extensive resonance overlap exacerbates assignment of intrinsically disordered proteins (IDPs). This issue can be circumvented by utilizing ^{15}N, $^{13}C'$ and $^{1}H^{N}$ spins, where the chemical shift dispersion is mainly dictated by the characteristics of consecutive amino acid residues. Especially ^{15}N and $^{13}C'$ spins offer superior chemical shift dispersion in comparison to $^{13}C^{\alpha}$ and $^{13}C^{\beta}$ spins. However, HN-detected experiments suffer from exchange broadening of amide proton signals on IDPs especially under alkali conditions. To that end, we propose here two novel HA-detected experiments, (HCA)-CON(CA)H and (HCA)NCO(CA)H and a new assignment protocol based on panoply of unidirectional HA-detected experiments that enable robust backbone assignment of IDPs also at high pH. The new approach was tested at pH 6.5 and pH 8.5 on cancer/testis antigen CT16, a 110-residue IDP, and virtually complete backbone assignment of CT16 was obtained by employing the novel HA-detected experiments together with the previously introduced iH(CA)NCO scheme. Remarkably, also those 10 N-terminal residues that remained unassigned in our earlier HN-detection based assignment approach even at pH 6.5 were now readily assigned. Moreover, theoretical calculations and experimental results suggest that overall sensitivity of the new experiments is also applicable to small or medium sized globular proteins that require alkaline conditions.

S. Mäntylahti · M. Hellman · P. Permi (✉)
Program in Structural Biology and Biophysics, NMR Laboratory, Institute of Biotechnology, University of Helsinki, P.O. Box 65, 00014 Helsinki, Finland
e-mail: Perttu.Permi@helsinki.fi

Keywords Assignment · CT16 · HA-detection · (HCA)CON(CA)H · (HCA)NCO(CA)H · Intrinsically disordered proteins · IDP

Introduction

Studies of intrinsically unfolded proteins (IDPs) by solution state NMR spectroscopy has extended our understanding of the complex interplay between the structure, dynamics and function (Dyson and Wright 2001, 2005). Biophysical characterization of IDPs is particularly amenable to NMR studies as rapid interconversion between various conformers sustains relatively long transverse relaxation times even on relatively long polypeptide chains. The negative implication of this conformational sampling is averaging of NMR chemical shifts, which are weighted average of various conformers in the ensemble. Thus far, any detailed structural study by NMR necessitates full or nearly complete assignment of protein resonances. In principle, for IDPs this task can be accomplished with a set of experiments that offer high resolution that helps in distinguishing between minute chemical shift differences between alike spins. A typical assignment approach involves a suite of HN-detected experiments, which are conceptually similar to those used for the assignment of globular proteins (for review, see e.g., Sattler et al. 1999; Permi and Annila 2004). However, in case of IDPs, carbonyl carbon ($^{13}C'$) rather than alpha carbon ($^{13}C^{\alpha}$) is routinely employed with nitrogen (^{15}N) to the assignment procedure due to its superior chemical shift dispersion (Yao et al. 1997). We have been developing and applying successfully HN-detected intra-residual experiments for the assignment of IDPs (Permi 2002; Tossavainen and Permi 2004; Alho et al. 2007; Mäntylahti et al. 2009). While sequential assignment

procedure based on HN-detection has been an undisputed success story for globular proteins and has extended the attainable molecular weight amenable NMR studies through deuteration (Yamazaki et al. 1994) and TROSY spectroscopy (Pervushin et al. 1997), it has properties that render it less suitable for the assignment of IDPs. Firstly, under alkali conditions (pH $\geq$ 7) labile amide protons are exposed to solvent and exchange rapidly with water, resulting in broadened HN resonances with consequent decrease in sensitivity and resolution (Bai et al. 1993; Grzesiek et al. 1997; Hu et al. 2007). This becomes especially pronounced in case of IDPs, in which the stabilizing amide proton hydrogen bonding is far less abundant. Secondly, many IDPs are composed of proline-rich polypeptide segments (Marsh and Forman-Kay 2010) and sequential assignment of N-substituted residues is a challenge in structural characterization of IDPs with polyproline stretches. Earlier proposed HCAN/(HB)CBCA(CO)N(CA)HA (Kanelis et al. 2000) and proline-optimized CDCA(NCO)-CAHA (Bottomley et al. 1999), as well as recently introduced $^{13}C'$-detected experiments (Bermel et al. 2006, 2009) are not ideal for the assignment of IDPs as they rely on poorly dispersed $^{13}C^{\alpha}$ chemical shifts and/or create unnecessary cross-peak overlap due to bidirectional coherence transfer. To that end, we recently introduced a set of HA-detected experiments, which establish the sequential linking in disordered polypeptides by correlating solely $^{15}N(i)$ or $^{15}N(i+1)$ chemical shifts with $^{13}C'(i)$ and $^{1}H^{\alpha}(i)$ spins in three-dimensional iH(CA)NCO and H(CA)CON spectra (Mäntylahti et al. 2010). However, degenerate ^{15}N chemical shifts occur frequently in IDPs and we propose here an extended approach where the sequential linkages are obtained via intraresidual and sequential $^{13}C'$ resonances. We dub the experiments proposed here as (HCA)-CON(CA)H and (HCA)NCO(CA)H, which can be used concomitantly with iH(CA)NCO for the efficient backbone assignment of IDPs. Indeed, we have successfully employed this assignment protocol to cancer/testis antigen CT16, a 110-residue intrinsically unstructured protein. In addition, performance of the proposed experiments with respect to the existing methodology was evaluated both by theoretical calculations and experimental data measured on small globular Ig-binding B1 domain of protein G (GB1).

Results and discussion

Description of the pulse sequences: (HCA)CON(CA)H

Figure 1a and b display excerpts of protein backbone and magnetization transfer pathways utilized by the novel (HCA)CON(CA)H and (HCA)NCO(CA)H experiments. Let us first focus on the (HCA)CON(CA)H scheme in Fig. 1c. The coherence flows through the (HCA)-CON(CA)H experiment in the following way:

$$\begin{aligned} &^{1}H^{\alpha}(i-1) \xrightarrow{^{1}J_{H^{\alpha}C^{\alpha}}} {}^{13}C^{\alpha}(i-1) \xrightarrow{^{1}J_{C^{\alpha}H^{\alpha}};^{1}J_{C^{\alpha}C'}} {}^{13}C'(i-1)\left[2T_A - t_1; {}^{1}J_{C'N}\right] \\ &\rightarrow {}^{15}N(i)\left[2T_{NC} - t_2; {}^{1}J_{C'N}, {}^{1}J_{C^{\alpha}N}, {}^{2}J_{C^{\alpha}N}\right] \\ &\rightarrow {}^{13}C^{\alpha}(i) \xrightarrow{^{1}J_{C^{\alpha}H^{\alpha}};^{1}J_{C^{\alpha}N}} {}^{1}H^{\alpha}(i)[t_3] \end{aligned} \quad (1)$$

Active couplings involved in coherence transfer are indicated above the arrows and inside square brackets, whereas t_i (i = 1–3) refers to the acquisition time for the corresponding spin. In essence, the (HCA)CON(CA)H experiment is a new HA-detected implementation of the famous HN(COCA)NH scheme (Weisemann et al. 1993; Grzesiek et al. 1993) and its derivatives (Matsuo et al. 1996; Bracken et al. 1997; Panchal et al. 2001; Sun et al. 2005; Fiorito et al. 2006). Experiment starts with the ^{1}H–^{13}C INEPT for transferring the $^{1}H(i-1)$ spin polarization to directly bound $^{13}C^{\alpha}(i-1)$ spin (Morris and Freeman 1979). The coherence is relayed to the $^{13}C'(i-1)$ spin using the Shaka-6 composite pulse, which simultaneously refocuses $^{13}C^{\alpha}$ resonances and inverts $^{13}C'$ resonances (Shaka 1985). At the same time, the antiphase ^{1}H–^{13}C coherence will be refocused during the delay τ_2. This delay should optimally be set to 3.4 ms, corresponding to $1/(2J_{CH})$, for IS spin moieties. However, this efficiently purges signals originating from I_2S spin systems (glycines), and consequently a compromise value of 2.4 ms should be used if simultaneous observation cross peaks stemming from the IS and I_2S spin systems are desired. At time point a, the magnetization can be described by the density operator

$$\sigma(a) = C_z^{\alpha}(i-1)C_y'(i-1) \quad (2)$$

During the ensuing period between time points a and b, the magnetization is simultaneously dephased by the $^{1}J_{C'N}$ scalar coupling during $2T_A$ and frequency labeled by the $^{13}C'(i-1)$ chemical shift during t_1. The following 90° pulses convert the desired coherence into ^{15}N coherence, described by the density operator (time point b)

$$\sigma(b) = C_z^{\alpha}(i-1)C_z'(i-1)N_y(i)\cos(\omega_{C'(i-1)}t_1) \quad (3)$$

The following delay $2T_{NC}$ is used for refocusing the magnetization with respect to $^{13}C^{\alpha}(i-1)$ and $^{13}C'(i-1)$ spins and dephasing it with respect to the $^{13}C^{\alpha}(i)$ spin. The second indirectly detected period (t_2) is used for labeling the $^{15}N(i)$ chemical shift, which is implemented in a constant time manner,. At time point c, after converting ^{15}N coherence into $^{13}C^{\alpha}$ coherence, the magnetization components can be described by the density operator

$$\begin{aligned} \sigma(c) = {} & N_z(i)C_y^{\alpha}(i)\cos(\omega_{C'(i-1)}t_1)\cos(\omega_{N(i)}t_2) + C_y^{\alpha}(i-1)N_z(i)\cos(\omega_{C'(i-1)}t_1)\cos(\omega_{N(i)}t_2) \end{aligned} \quad (4)$$

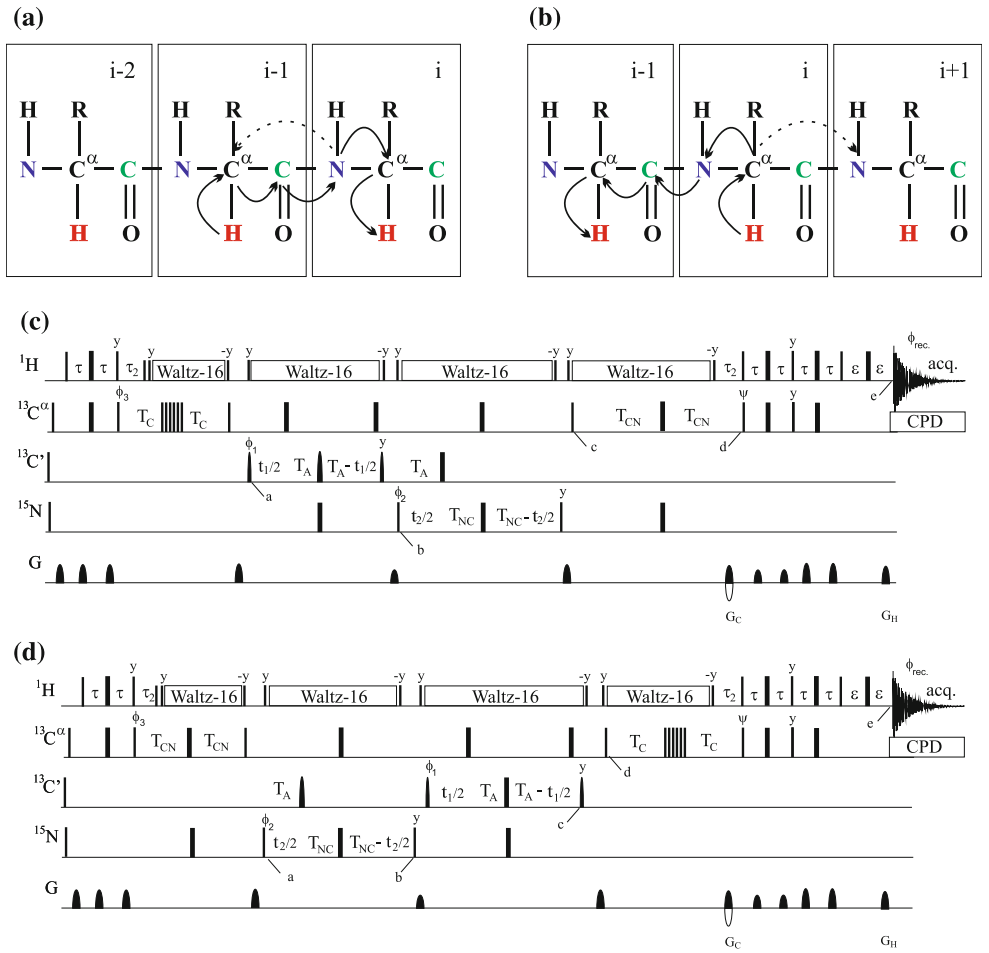

Fig. 1 Schematic presentation of magnetization transfer pathway during **a** the (HCA)CON(CA)H and **b** (HCA)NCO(CA)H experiments. *Arrows* with *solid line* indicate the actual magnetization transfer pathway, whereas an *arrow* with a *broken line* represents coherence transfer route which can be suppressed with an appropriate delay setting. **c** (HCA)CON(CA)H experiment for establishing correlations between $^{1}H^{\alpha}(i)$, $^{15}N(i)$, and $^{13}C'(i-1)$, and $^{1}H^{\alpha}(i-1)$, $^{15}N(i)$, and $^{13}C'(i-1)$ ($T_{NC} = 12$–15 ms) chemical shifts or solely $^{1}H^{\alpha}(i)$, $^{15}N(i)$, and $^{13}C'(i-1)$ chemical shifts ($T_{NC} = 25$ ms). **d** (HCA)NCO(CA)H experiment for correlating $^{1}H^{\alpha}(i-1)$, $^{13}C'(i-1)$ and $^{15}N(i)$ chemical shifts in uniformly ^{15}N, ^{13}C enriched proteins. Narrow and wide rectangles correspond to 90° and 180° flip angles, respectively. Pulses are applied with phase x unless otherwise indicated. The ^{1}H, ^{15}N, $^{13}C'$, and $^{13}C^{\alpha}$ carrier positions are 4.7 (water), 118 (center of ^{15}N spectral region), 175 ppm (center of $^{13}C'$ spectral region), and 57 ppm (center of $^{13}C^{\alpha}$ spectral region). The ^{13}C carrier is set initially to the middle of $^{13}C^{\alpha}$ region (57 ppm), shifted to 175 ppm prior to the first 90° $^{13}C'$ pulse (in (HCA)CON(CA)H time point *a* and (HCA)NCO(CA)H time point *b*), and shifted back to 57 ppm at the time point *c*. All rectangular 90° pulses for $^{13}C^{\alpha}$ (57 ppm) and 180° pulses for $^{13}C'$ (175 ppm) were applied with durations of 40.4 μs (90°) and 36.2 μs (180°) at 800 MHz, respectively, in order to provide null mutual excitation (Kay et al. 1990). The cascade of rectangular pulses on $^{13}C^{\alpha}$ denotes a composite pulse for ultra-broadband inversion with durations defined by pwC*(β_i/90), where β_i is a flip angle for individual pulses in the cascade i.e. 158.0, 171.2, 342.8, 145.5, 81.2, 85.3 (Shaka 1985). Selective 90° pulses for $^{13}C'$ have the shape of center lobe of a sinc function and duration of 66.8 μs at 800 MHz. Phase modulated 180° pulses, applied off-resonance for $^{13}C^{\alpha}$, have the shape of one-lobe sinc profile and duration of 60.4 μs. The Waltz-16 sequence (Shaka et al. 1983) with a strength of 4.8 kHz is employed to decouple ^{1}H spins during $2(T_{CN} + T_{NC} + T_A + T_C) - 2\tau_2$. The adiabatic WURST field (Kupće and Wagner 1995) was used to decouple ^{13}C during acquisition. Delay durations: $\tau = 1/(4J_{HC}) \sim 1.7$ ms; $\tau_2 = 3.4$ ms (optimized for non-glycine residues) or 2.2–2.5 ms (for observing both glycine and non-glycine residues); ε = duration of G_H + field recovery ~0.4 ms; $T_C = 1/(6J_{C\alpha C'}) \sim 3.4$ ms; $T_A = 1/(4J_{C'N}) \sim 16.6$ ms; $T_{CN} \sim 14$ ms. The $^{15}N \rightarrow {}^{13}C$ transfer delay T_{NC} is set to 25 ms to suppress the auto-correlated pathway or in (HCA)CON(CA)H to 12–15 ms for observing both sequential and auto-correlated cross-peaks. Maximum t_1 and t_2 are restrained in **c** $t_{1,max} < 2.0*T_A$, and $t_{2,max} < 2.0*T_{NC}$ and **d** $t_{1,max} < 2.0*T_A$ and $t_{2,max} < 2.0*T_{NC}$. Frequency discrimination in $^{13}C'$ and ^{15}N dimensions are obtained using the States-TPPI protocol (Marion et al. 1989) applied to ϕ_1 and ϕ_2, respectively. Phase cycling: ϕ_1 = x, −x; ϕ_2 = 2(x), 2(−x); ϕ_3 = 4(x), 4(−x); ψ = x; $\phi_{rec.}$ = x, 2(−x), x, −x, 2(x), −x. Gradient strengths and durations: G_C = 13 k G/cm (1.6 ms), G_H = 13 k G/cm (0.4 ms). The pulse sequences code and parameter file for Varian Inova system are available from authors website URL http://www.biocenter.helsinki.fi/bi/nmr/permi

Between the time points c and d, the coherence is refocused and dephased with respect to ^{15}N and $^{1}H^{\alpha}$, respectively. Finally, the density operator at time point d

$$\sigma(d) = H_z^{\alpha} C^{+}(i) \cos(\omega_{C'(i-1)} t_1) \cos(\omega_{N(i)} t_2) + H_z^{\alpha} C^{+}(i-1) \cos(\omega_{C'(i-1)} t_1) \cos(\omega_{N(i)} t_2) \quad (5)$$

will be converted into observable $^{1}H^{\alpha}$ coherence by the subsequent coherence order selective coherence transfer scheme (Kay et al. 1992; Schleucher et al. 1994). Thus, the observable magnetization at time point e

$$\sigma(e) = H^{-} \cos(\omega_{C'(i-1)} t_1) \cos(\omega_{N(i)} t_2) \exp(i\omega_{H(i)} t_3) + H^{-} \cos(\omega_{C'(i-1)} t_1) \cos(\omega_{N(i)} t_2) \exp(i\omega_{H(i-1)} t_3) \quad (6)$$

is frequency modulated by $^{13}C'(i-1)$, $^{15}N(i)$ and $^{1}H^{\alpha}(i)$, and $^{13}C'(i-1)$, $^{15}N(i)$ and $^{1}H^{\alpha}(i-1)$ chemical shifts during t_1, t_2 and t_3 periods, respectively. The first term in Eq. 6 corresponds to a sequential cross peak, whereas the latter term represents the auto-correlated peak.

The overall transfer function $I_{(HACA)CON(CA)HA}$ is for the sequential peak is proportional to

$$\begin{aligned} I_{seq} \approx & \sin(2\pi^1 J_{C\alpha N} T_{NC}) \sin(2\pi^2 J_{C\alpha N} T_{NC}) \sin(2\pi^1 J_{C'N} T_A) \\ & \sin(2\pi^1 J_{C'N} T_A) \sin(2\pi^1 J_{C\alpha C'} T_C) \cos(2\pi^1 J_{C\alpha C\beta} T_C) \\ & \sin(2\pi^1 J_{C\alpha N} T_{CN}) \cos(2\pi^2 J_{C\alpha N} T_{CN}) \cos(2\pi^1 J_{C\alpha C\beta} T_{CN}) \\ & \exp(-2(T_{CN} + T_C)/(T_{2,C\alpha})) \exp(-(2T_A)/(T_{2,C'})) \\ & \exp(-(2T_{NC})/(T_{2,N})) \end{aligned} \quad (7)$$

and for the auto-correlated peak

$$\begin{aligned} I_{auto} \approx & \cos(2\pi^1 J_{C\alpha N} T_{NC}) \cos(2\pi^2 J_{C\alpha N} T_{NC}) \\ & \sin(2\pi^1 J_{C'N} T_A) \sin(2\pi^1 J_{C'N} T_A) \sin(2\pi^1 J_{C\alpha C'} T_C) \\ & \cos(2\pi^1 J_{C\alpha C\beta} T_C) \cos(2\pi^1 J_{C\alpha N} T_{CN}) \sin(2\pi^2 J_{C\alpha N} T_{CN}) \\ & \cos(2\pi^1 J_{C\alpha C\beta} T_{CN}) \exp(-2(T_{CN} + T_C)/(T_{2,C\alpha})) \\ & \exp(-(2T_A)/(T_{2,C'})) \exp(-(2T_{NC})/(T_{2,N})) \end{aligned} \quad (8)$$

In Eqs. 7 and 8, $^{1}J_{C\alpha C'}$, $^{1}J_{C'N}$ and $^{1}J_{C\alpha C\beta}$ correspond to values of 53, 15 and 35 Hz i.e. one-bond J couplings for $^{13}C^{\alpha}$–$^{13}C'$, $^{13}C'$–^{15}N and $^{13}C^{\alpha}$–$^{13}C^{\beta}$, respectively. The average random coil values for one-bond ($^{1}J_{C\alpha N}$) and two-bond ($^{2}J_{C\alpha N}$) couplings between backbone $^{13}C^{\alpha}$ and ^{15}N spins are 10.6 Hz and 7.5 Hz, respectively (Delaglio et al. 1991). Depending on delay setting utilized for $^{15}N \rightarrow {}^{13}C^{\alpha}$ transfer during $2T_{NC}$, the intensities of sequential and auto-correlated peaks can be modulated (Panchal et al. 2001). Therefore, sequential and auto-correlated cross peaks will have 180° phase difference, which can be utilized during the assignment procedure. It is noteworthy that accidental overlap of sequential and auto-correlated cross peaks is inevitable in the case of IDPs, and it can hamper the recognition of sequential connectivities. However, by setting the delays T_{NC} and T_A (between time points b and c) to ~25 ms and 16.6 ms, respectively, the intensity of the sequential peaks can be maximized while the outbreak of the auto-correlated peaks is minimized. This implementation establishes the first order intraresidual filter (Permi 2002; Fiorito et al. 2006; Mäntylahti et al. 2009). In this way, the auto-correlated pathway is efficiently suppressed and unnecessary spectral overlap can be minimized.

We considered theoretical coherence transfer efficiencies for the sequential and auto-correlated cross peaks and compare the results with the existing pulse sequences. To this end, we consider an IDP with average transverse relaxation times of 200, 100 and 200 ms for ^{15}N, $^{13}C^{\alpha}$ and $^{13}C'$ spins, respectively. After numerical optimization of transfer delays T_C (~3.25 ms), T_A (~16 ms), T_{NC} (~12.5 ms) and T_{CN} (~28 ms), we get transfer efficiencies of 0.092 and −0.072 for the sequential and auto-correlated peaks, respectively. Analogously, by setting the delay T_{NC} to 25 ms, one obtains transfer efficiencies of 0.181 and 0.004 for the sequential and auto-correlated cross peaks, respectively. Thus, setting the delay T_{NC} ~ 25 ms, the transfer efficiency for the sequential pathway improves by a factor 2 while the auto-correlated pathway is practically suppressed. Similar linkage between $^{13}C'(i-1)$, $^{15}N(i)$, $^{1}H^{\alpha}(i)$ spins can be obtained using the HCA(N)CO experiment originally described by Yamazaki et al. (1997) and recently revisited by Ogura et al. (2010). In this case, the original pulse scheme should be modified for recording ^{15}N chemical shift instead of $^{13}C^{\alpha}$. In H(CA)NCO pulse scheme, magnetization is transferred from $^{1}H^{\alpha}$ spin to the intraresidual and sequential $^{13}C'$ spins via $^{1}H^{\alpha} \rightarrow {}^{13}C^{\alpha} \rightarrow {}^{15}N \rightarrow {}^{13}C'$ pathway in an out-and-back manner. Theoretical calculations suggest that the novel (HCA)CON(CA)H scheme proposed here provides subtle increase in attainable sensitivity (~10%) with respect to the H(CA)NCO experiment for IDPs under conditions described above. However, as the molecule size increases, differences in relative intensities between the experiments become evident. In case of medium sized globular proteins, the relative intensity of (HCA)-CON(CA)H is 50%, 40% and 65% higher in comparison to H(CA)NCO for residues in random coil, α-helical, or extended conformation, respectively. Figure 2 shows theoretical coherence transfer efficiencies for (HCA)-CON(CA)H and H(CA)NCO experiments on globular proteins with effective rotational correlation time of ~8 ns. More importantly, and especially pronounced on the assignment IDPs, the (HCA)CON(CA)H experiment offers twofold increase in attainable resolution by eliminating redundant cross peaks emerging through the auto-correlated pathway.

Finally, $^{13}C'$-detected experiments introduced by Bermel and co-workers have been shown to be highly

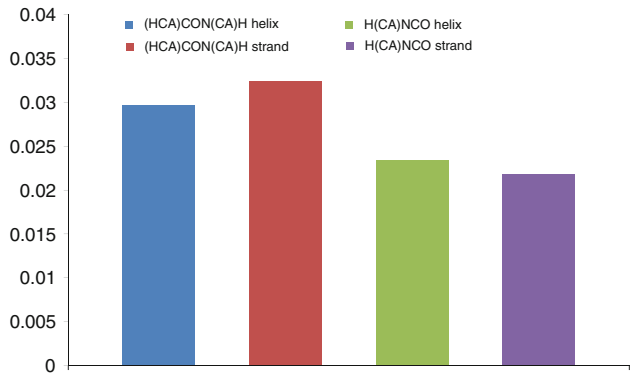

Fig. 2 Theoretical coherence transfer efficiency for sequential $^{13}C'(i-1)$–$^{1}H^{\alpha}(i)$ correlations in the novel (HCA)CON(CA)H and H(CA)NCO experiments (Yamazaki et al. 1994; Ogura et al. 2010). Calculations were carried out using $^{1}J_{NC\alpha}$ and $^{2}J_{NC\alpha}$ values earlier reported for residues in α-helix ($^{1}J_{NC\alpha} = 9.6$ Hz and $^{2}J_{NC\alpha} = 6.4$ Hz) and β-strand ($^{1}J_{NC\alpha} = 10.9$ Hz and $^{2}J_{NC\alpha} = 8.3$ Hz) (Delaglio et al. 1991). The corresponding transverse relaxation times of 60, 30 and 60 ms for ^{15}N, $^{13}C^{\alpha}$ and $^{13}C'$ spins were assumed, respectively. Additional parameters used in simulation were $^{1}J_{C\alpha C'} = 53$ Hz, $^{1}J_{C\alpha C\beta} = 35$ Hz, and $^{1}J_{NC'} = 15$ Hz

useful for the assignment of IDPs (Bermel et al. 2009). The $^{13}C'$-detected (H)CANCO experiment offers the coherence transfer efficiency (~0.21 for sequential pathway) comparable to (HCA)CON(CA)H (~0.18). However, the experiments based on $^{13}C'$-detection suffer from eightfold sensitivity loss in comparison to ^{1}H-detected experiments. In the case of HA-detection, this difference will be counterbalanced by up to fourfold sensitivity loss due to doublet of doublets (in D_2O) nature of HA resonances owing to homonuclear three-bond couplings to Hβ's, in residues other than Gly, Ile, Thr, Val. Therefore theoretical calculations suggest that the proposed (HCA)CON(CA)H offers ca. 2 times higher sensitivity than the corresponding (H)CANCO scheme (Bermel et al. 2009).

Description of the pulse sequences: (HCA)NCO(CA)H

A complementary (HCA)NCO(CA)H experiment, shown in Fig. 1d, utilizes similar but reverse coherence transfer route in comparison to (HCA)CON(CA)H:

$$\begin{aligned} &^{1}H^{\alpha}(i) \xrightarrow{^{1}J_{H^{\alpha}C^{\alpha}}} {}^{13}C^{\alpha}(i) \xrightarrow{^{1}J_{C^{\alpha}H^{\alpha}};^{1}J_{C^{\alpha}N}} {}^{15}N(i) \\ &\left[2T_{NC} - t_2; {}^{1}J_{C'N}, {}^{1}J_{C^{\alpha}N}; {}^{2}J_{C^{\alpha}N}\right] \rightarrow {}^{13}C'(i-1) \\ &\left[2T_A - t_1; {}^{1}J_{C'N}\right] \rightarrow {}^{13}C^{\alpha}(i-1) \xrightarrow{^{1}J_{C^{\alpha}H^{\alpha}};^{1}J_{C^{\alpha}C'}} {}^{1}H^{\alpha}(i-1)[t_3] \end{aligned} \quad (9)$$

Again, the magnetization is first transferred from $^{1}H^{\alpha}(i)$ to $^{13}C^{\alpha}(i)$ as in (HCA)CON(CA)H experiment, but instead of relaying magnetization to ^{15}N through $^{13}C'$ spin, it is directly transferred from $^{13}C^{\alpha}(i)$ to $^{15}N(i)$ and $^{15}N(i+1)$, which can be described by the density operator (time point *a*):

$$\sigma(a) = C_z^{\alpha}(i)N_y(i) + C_z^{\alpha}(i)N_y(i+1) \quad (10)$$

It is noteworthy that the coherence will be transferred to both intraresidual and sequential nitrogens, but the pathway leading to the auto-correlated cross peak will be almost completely suppressed by setting the $T_{NC} = \sim 25$ ms as in the case of (HCA)CON(CA)H experiment (vide supra). During the ensuing $2T_{NC}$ and $2T_A$ time periods (between time points *a* and *b*), the magnetization will be refocused and dephased with respect to $^{13}C^{\alpha}(i)$ and $^{13}C^{\alpha}(i-1)$ spins, and dephased with respect $^{13}C'(i-1)$ spin. The ^{15}N chemical shift labeling takes place during the t_2 period, implemented into the $2T_{NC}$ period, which yields very high resolution in ^{15}N dimension. Hence the spin system at time point *b* can be described by the density operator:

$$\begin{aligned} \sigma(b) = {} & N_x(i)C_z'(i-1)C_z^{\alpha}(i-1)\cos(\omega_{N(i)}t_2) \\ & + C_z^{\alpha}(i)C_z'(i)N_x(i+1)\cos(\omega_{N(i+1)}t_2) \end{aligned} \quad (11)$$

The ^{15}N chemical shift labeling is followed by the chemical shift evolution of $^{13}C'(i-1)$ spin during t_1 with concomitant refocusing of the $^{13}C'$ antiphase coherence with respect to ^{15}N during $2T_A$, and the spin system can be described by the density operator at time point *c*.

$$\begin{aligned} \sigma(c) = {} & C_x'(i-1)C_z^{\alpha}(i-1)\cos(\omega_{N(i)}t_2)\cos(\omega_{C(i-1)}t_1) \\ & + C_z^{\alpha}(i)C_x'(i)\cos(\omega_{N(i+1)}t_2)\cos(\omega_{C(i)}t_1) \end{aligned} \quad (12)$$

Subsequently, the desired magnetization will be converted into the antiphase $^{13}C^{\alpha}$ coherence at time point *d*:

$$\begin{aligned} \sigma(d) = {} & C_y^{\alpha}(i-1)\cos(\omega_{N(i)}t_2)\cos(\omega_{C(i-1)}t_1) \\ & + C_y^{\alpha}(i)\cos(\omega_{N(i+1)}t_2)\cos(\omega_{C(i)}t_1) \end{aligned} \quad (13)$$

The observable magnetization at time point *e* corresponds to:

$$\begin{aligned} \sigma(e) = {} & H^{-}\cos(\omega_{N(i)}t_2)\cos(\omega_{C(i-1)}t_1)\exp(i\omega_{H^{\alpha}(i-1)}t_3) \\ & + H^{-}\cos(\omega_{N(i+1)}t_2)\cos(\omega_{C(i)}t_1)\exp(i\omega_{H^{\alpha}(i)}t_3) \end{aligned} \quad (14)$$

The first operator corresponds to the desired magnetization, which has modulated by $^{13}C'(i-1)$, $^{15}N(i)$ and $^{1}H^{\alpha}(i-1)$ chemical shift during t_1, t_2 and t_3, respectively. The latter term corresponds to the magnetization, which has modulated by $^{13}C'(i)$, $^{15}N(i+1)$, and $^{1}H^{\alpha}(i)$ chemical shifts during t_1-t_3, but which has strongly suppressed by setting the delay T_{NC} (= ~25 ms). Hence, after Fourier transform a cross peak will emerge at coordinates $\omega_{N(i)}$, $\omega_{C'(i-1)}$, $\omega_{H\alpha(i-1)}$.

The coherence transfer functions for the sequential and auto-correlated cross peaks in the (HCA)NCO(CA)H scheme are identical to those of (HCA)CON(CA)H because in essence both experiments utilize identical but reverse coherence transfer pathway. Consequently, the

theoretical coherence transfer efficiencies for (HCA)-CON(CA)H and (HCA)NCO(CA)H experiments are identical. However, few practical features differ between these two experiments, which call for a more detailed explanation. First, the sign of the glycine residues in the (HCA)-CON(CA)H experiment deviate 180° from others amino acids, because during the final $^{15}N \rightarrow {}^{13}C^{\alpha}$ refocusing INEPT ($2T_{CN} \sim 25$–28 ms), signal will be modulated by $\cos(2\pi J_{C\alpha C\beta} T_{CN})$ for all but glycine residue. In addition, in the (HCA)NCO(CA)H experiment, the residue preceding the glycine exhibits a 180° phase difference with respect to any other residue. This can be realized by noting that $\cos(2\pi J_{C\alpha C\beta} T_{CN})$ modulation, in consecutively linked dipeptide units, will have effect on the residue from which the magnetization originates. It is therefore easy to utilize this sign information during the sequential assignment process to facilitate identification of glycines as well as those residues that precede glycines.

The next point of interest concerns proline residues. The coherence transfer function given in Eq. 7 should now include additional term, $\cos(2\pi J_{NC\delta} T_{NC})$, due to extraordinary chemical structure of proline residue. As an N-substituted amino acid, the side-chain $^{13}C\delta$ spin replaces the ^{15}N bound amide proton in proline, and thereby additional one-bond coupling between ^{15}N–$^{13}C\delta$ modulates the signal amplitude during $2T_{NC}$. Hence, the first line in Eq. 7 becomes

$$I_{seq.}^{non-pro} \approx \sin(2\pi^1 J_{C\alpha N} T_{NC}) \sin(2\pi^2 J_{C\alpha N} T_{NC}) \sin(2\pi^1 J_{C'N} T_A) \quad (15)$$

and

$$I_{seq.}^{pro} \approx \sin(2\pi^1 J_{C\alpha N} T_{NC}) \cos(2\pi^1 J_{C\delta N} T_{NC}) \sin(2\pi^2 J_{C\alpha N} T_{NC}) \sin(2\pi^1 J_{C'N} T_A) \quad (16)$$

for non-proline and proline residues. By setting $T_{NC} = 25$ ms yields coherence transfer efficiency of 0.92 and 0.087 for non-proline and proline residues, assuming $^1J_{NC\alpha}$, $^2J_{NC\alpha}$ and $^1J_{NC\delta}$ of 10.6, 7.5 and 10.5 Hz, respectively.

Alternative approach to obtain sequential $\omega_{N(i)}$, $\omega_{C'(i-1)}$, $\omega_{H\alpha(i-1)}$ connectivities is to utilize H(CA)CON experiment (Mäntylahti et al. 2010). In this scheme, the magnetization is transferred from the $^1H^{\alpha}$ spin of residue $i-1$ to the ^{15}N spin of the following residue i using the $^1H^{\alpha} \rightarrow {}^{13}C^{\alpha} \rightarrow {}^{13}C' \rightarrow {}^{15}N$ pathway in an out-and-back –type experiment. Although the coherence transfer efficiency of the H(CA)CON experiment ($I_{seq.} \sim 0.29$) is far superior to the (HCA)NCO(CA)H experiment ($I_{seq.} \sim 0.18$), the latter provides few advantages. Firstly, the sign information available in the (HCA)NCO(CA)H experiment facilitates the assignment procedure especially on natively unfolded proteins. Secondly, at the highest magnetic field, $^{13}C'$ CSA deteriorates sensitivity of the H(CA)CON experiment due to long transfer steps needed for transferring magnetization from $^{13}C'$ to ^{15}N and back. Moreover, the attainable sensitivity of the (HCA)NCO(CA)H experiment with respect to H(CA)CON will be further counterbalanced by dissolving the protein into D_2O and by employing ^2H decoupling for removal of J-coupling interaction between ^{15}N and ^2H during the $^{15}N \rightarrow {}^{13}C$ transfer step ($2T_{NC}$) in (HCA)NCO(CA)H experiment.

(HCA)CON(CA)H and (HCA)NCO(CA)H experiments can be expanded into 4D experiments by establishing correlations between $^{13}C'(i-1)$, $^{15}N(i)$, $^{13}C^{\alpha}(i)$, $^1H^{\alpha}(i)$ and $^{15}N(i)$, $^{13}C'(i-1)$, $^{13}C^{\alpha}(i-1)$, $^1H^{\alpha}(i-1)$. In that case, effective resolution in $^{13}C^{\alpha}$ dimension of the (HCA)NCO-CAH experiment is limited to $2T_C$, which is typically set to 6.5–7 ms as a compromise between $^{13}C^{\alpha}$ spin relaxation rate, and active and passive J couplings between $^{13}C'$–$^{13}C^{\alpha}$ and $^{13}C^{\alpha}$–$^{13}C^{\beta}$. This may not be highly beneficial in case of IDPs, where the chemical shift dispersion is very limited in $^{13}C^{\alpha}$ dimension. Alternatively, $2T_C$ can be extended to 27–28 ms, which in case of IDPs offers even increased coherence transfer efficiency ($I \sim 0.22$) by assuming $T_{2,C\alpha} \sim 100$ms. However, in the case of 15 kDa globular protein, this results in substantial decrease in overall sensitivity (50%). Nevertheless, as coherence order selective coherence transfer is already employed to $^{13}C^{\alpha} \rightarrow {}^1H^{\alpha}$ transfer for improved water suppression, this does not induce additional sensitivity loss with respect to 3D experiments (Kay et al. 1992; Schleucher et al. 1994).

Combination of (HCA)CON(CA)H, iH(CA)NCO, and (HCA)NCO(CA)H/H(CA)CON experiments offers efficient assignment protocol for IDPs and/or globular proteins which require alkali (pH > 7) conditions. Figure 3 shows schematically an assignment strategy that utilizes unidirectional coherence transfer available through these experiments. First, cross-peaks for intraresidual amide nitrogen, carbonyl and α-proton (N_i, C'_i, H^{α}_i) appear in iH(CA)NCO spectrum (Mäntylahti et al. 2010). By selecting the corresponding ^{15}N-plane of each spectra, the $N_i, C'_{i-1}, H^{\alpha}_i$ cross-peak in (HCA)CON(CA)H, and $N_i, C'_{i-1}, H^{\alpha}_{i-1}$ cross-peak in (HCA)NCO(CA)H enables the assignments of the resonances of carbonyl and α-proton of the preceding amino acid residue (marked as red spot and arrow). Intraresidual correlation of the residue N_{i-1} ($N_{i-1}, C'_{i-1}, H^{\alpha}_{i-1}$) in iH(CA)NCO appears at the corresponding C'_{i-1} projection and H^{α}_{i-1} frequency to (HCA)NCO(CA)H spectrum.

Application to streptococcal protein G and intrinsically disordered CT16

The novel pulse sequences were exposed to experimental verification on two proteins, an extensively studied 56-residue immunoglobulin-binding domain B1 of streptococcal

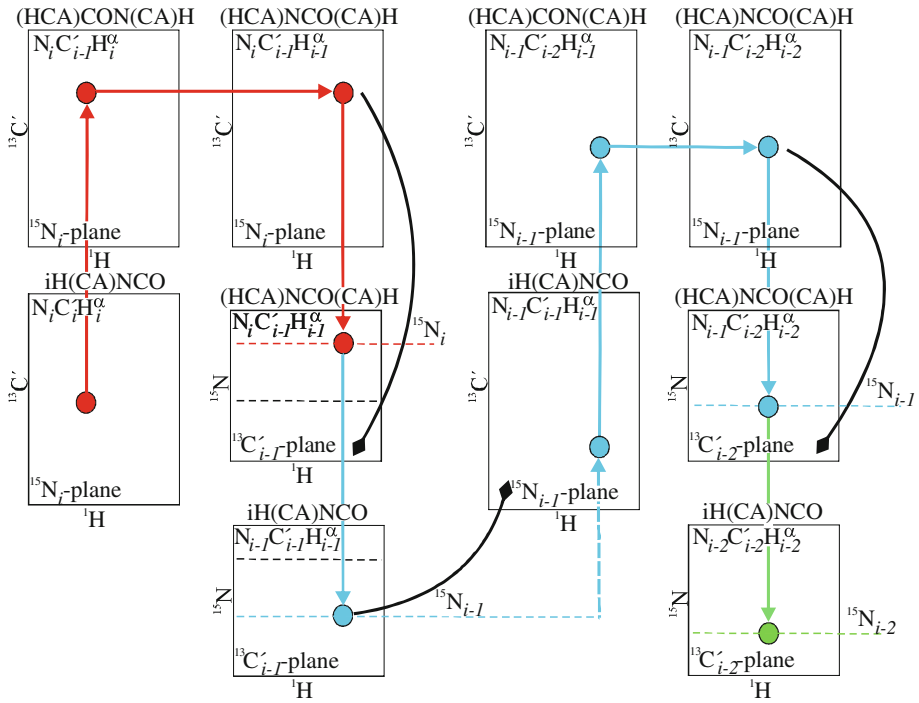

Fig. 3 Schematic presentation of sequential assignment procedure based on iH(CA)NCO (Mäntylahti et al. 2010), and novel (HCA)CON(CA)H and (HCA)NCO(CA)H (or alternatively H(CA)CON; Mäntylahti et al. 2010) spectra. Cross peaks resonating at the nitrogen frequency of the residues i, $i-1$ and $i-2$ are color-coded with *red*, *blue* and *green*, respectively

protein G (GB1), and cancer/testis antigen CT16 also recognized as PAGE5 belonging to Xage protein superfamily. GB1 is a small globular protein, composed of four antiparallel β-strands and one α-helix. CT16 has been found to be expressed in lung and renal cancers as well as in melanomas (Rappu et al. 2010). CT16 is a 110-residue protein belonging to the group of IDPs according to analysis of its amino acid composition by IUPred algorithm (http://iupred.enzim.hu) (Dosztányi et al. 2005) as well as ^{1}H, ^{13}C and ^{15}N chemical shift data. Therefore evaluation of overall performance of the proposed pulse sequences on GB1 and CT16 yields comparative insight into applicability of new experiments.

Figure 4 displays two-dimensional $^{1}H^{\alpha}$, $^{13}C'$ panels from GB1, recorded with the novel (HCA)CON(CA)H pulse scheme using $^{15}N \rightarrow {}^{13}C$ transfer delay $T_{NC} = 15$ ms (Fig. 4a) and $T_{NC} = 25$ ms (Fig. 4b). The corresponding two-dimensional $^{1}H^{\alpha}$–$^{13}C'$ correlation map recorded with the H(CA)NCO experiment is shown in Fig. 4c. The salient features of these experiments are clearly visible in these two-dimensional plots: (HCA)CON(CA)H ($T_{NC} = 15$ ms) and H(CA)NCO spectra exhibit both $^{1}H^{\alpha}(i)$–$^{13}C'(i-1)$ and $^{1}H^{\alpha}(i)$–$^{13}C'(i)$ correlations, whereas solely $^{1}H^{\alpha}(i)$–$^{13}C'(i-1)$ correlations are visible in the (HCA)CON(CA)H ($T_{NC} = 25$ ms) spectrum. The difference between (HCA)CON(CA)H ($T_{NC} = 15$ ms) and H(CA)NCO spectra is the sign discrimination between $^{1}H^{\alpha}(i)$–$^{13}C'(i-1)$ (red contours) and $^{1}H^{\alpha}(i)$–$^{13}C'(i)$ (blue contours) cross-peaks in the former. In addition, the glycine residues in both (HCA)CON(CA)H spectra (Fig. 4a, b) can be recognized by their phase difference in comparison to other residues. We compared the sensitivity of the new (HCA)CON(CA)H experiment with the H(CA)NCO scheme on GB1 at 30°C. The histogram in Fig. 5 shows measured peak heights for well-resolved sequential $^{13}C'(i-1)$, $^{1}H(i)$ cross peaks in GB1. Generally, the (HCA)CON(CA)H experiment with the $^{15}N \rightarrow {}^{13}C^{\alpha}$ transfer delay T_{NC} set to 25 ms, is 40% more sensitive than the H(CA)NCO experiment derived from the original HCA(N)CO schemes (Yamazaki et al. 1997; Ogura et al. 2010), and 30% more sensitive than the (HCA)-CON(CA)H scheme with $T_{NC} = 15$ ms. This is in good accordance with theoretical calculations for the protein of this size.

Assignment of IDPs is seriously hampered by the poor chemical shift dispersion especially on $^{13}C^{\alpha}$ and $^{13}C^{\beta}$ spins. Although we have successfully employed the HA-detection based strategy for the backbone assignment of the fifth 47-residue repeat of $EspF_U$ using the intraresidual iH(CA)NCO and sequential H(CA)CON schemes that link consecutive residues through ^{15}N chemical shift (Mäntylahti et al. 2010). However, in the case of CT16, the amount of cross-peak overlap is significantly more severe, which rendered the ^{15}N chemical shift based assignment difficult. To address this issue, we propose to use the novel (HCA)CON(CA)H experiment together with (HCA)N-CO(CA)H (or alternatively H(CA)CON) and iH(CA)NCO schemes. We applied these three experiments for the backbone assignment of CT16 using the protocol shown in Fig. 3. With this approach, we were able to accomplish a

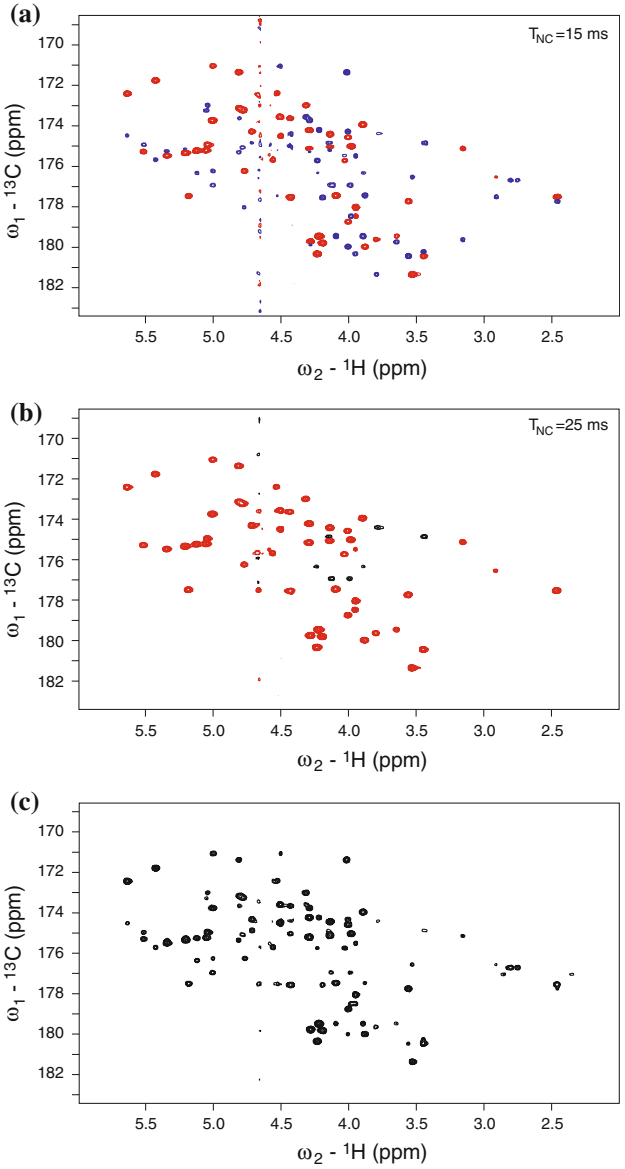

Fig. 4 Expansions of two-dimensional $^{13}C'$–^1H correlation map from GB1. Panel **a** displays $^{13}C'(i-1)$–$^1H(i)$ and $^{13}C'(i)$–$^1H(i)$ correlations with *red* and *blue* contours, respectively. The spectrum was recorded with the pulse scheme shown in Fig. 1c, using the $^{15}N \rightarrow {}^{13}C$ transfer delay set to $T_{NC} = 15$ ms. The spectrum in panel **b** shows solely sequential $^{13}C'(i-1)$–$^1H(i)$ connectivities, which were recorded with the (HCA)CON(CA)H pulse scheme using the delay setting $T_{NC} = 25$ ms. This effectively suppresses the auto-correlation pathway leading to $^{13}C'(i)$–$^1H(i)$ correlations. Spectrum in panel **c** represents two-dimensional H(CAN)CO correlation map, which shows both $^{13}C'(i-1)$–$^1H(i)$ and $^{13}C'(i)$–$^1H(i)$ cross-peaks. In comparison to the spectrum in panel **a**, the sequential and auto-correlated cross-peaks have identical phase properties. All spectra were recorded and processed with identical parameters, and are shown with identical contour levels, using a spacing factor of 1.4, which enables direct comparison of attainable sensitivities

nearly complete backbone assignment of CT16 at two different pHs: 6.5 and 8.5. Remarkably, we were able to obtain all the previous assignments and additionally assign

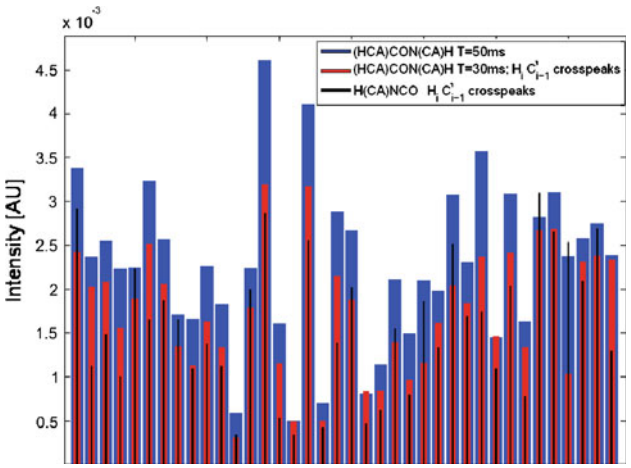

Fig. 5 Comparison of intensities for the sequential $^{13}C'(i-1)$–$^1H(i)$ cross-peaks between (HCA)CON(CA)H ($T_{NC} = 15$ ms) (*red bars*), (HCA)CON(CA)H ($T_{NC} = 25$ ms) (*blue bars*) and H(CA)NCO spectra (*black bars*). Intensities were measured for those $^{13}C'(i-1)$–$^1H(i)$ correlations in GB1, which were well-resolved and free from partial cross-peak overlap or potential disruption of residual water signal

N-terminal stretches G1-H6 and S10-S13 as well as all the prolines that remained unassigned in our HN-detection based approach either due to exchange broadening or inherent lack of HN proton in proline residues. Only resonances belonging to residues E36 and D100 remained unassigned. Figure 6 highlights the "sequential walk" for the stretch G1–S2–M3–S4–E5, which we were not able to assign using our HN-detected approach based on i(HCA)-CO(CA)NH and HNCO experiments even at moderately low pH 6.5 (Mäntylahti et al. 2009). Figure 7 displays ^{15}N HSQC spectra of CT16 measured at pH 6.5 (upper panel) and 8.5 (lower panel). Although exchange broadening of NH signals is clearly visible at alkali conditions, the assignment of ^1HA, $^{13}C'$ and ^{15}N signals is still possible using the iH(CA)NCO, (HCA)CON(CA)H and (HCA)N-CO(CA)H spectra as demonstrated in panels on the right.

Conclusions

We have presented novel and efficient assignment protocol based on HA-detection and unidirectional coherence transfer available in (HCA)CON(CA)H and (HCA)NCO(-CA)H experiments. Together with the unidirectional iH(CA)NCO experiment introduced earlier (Mäntylahti et al. 2010), these experiments provide robust platform for backbone assignment of natively unfolded proteins.

We demonstrated assignment protocol on cancer/testis antigen CT16, a 110-residue IDP, where nearly complete backbone assignment was obtained, including 10 N-terminal residues that remained unassigned in our HN-detection

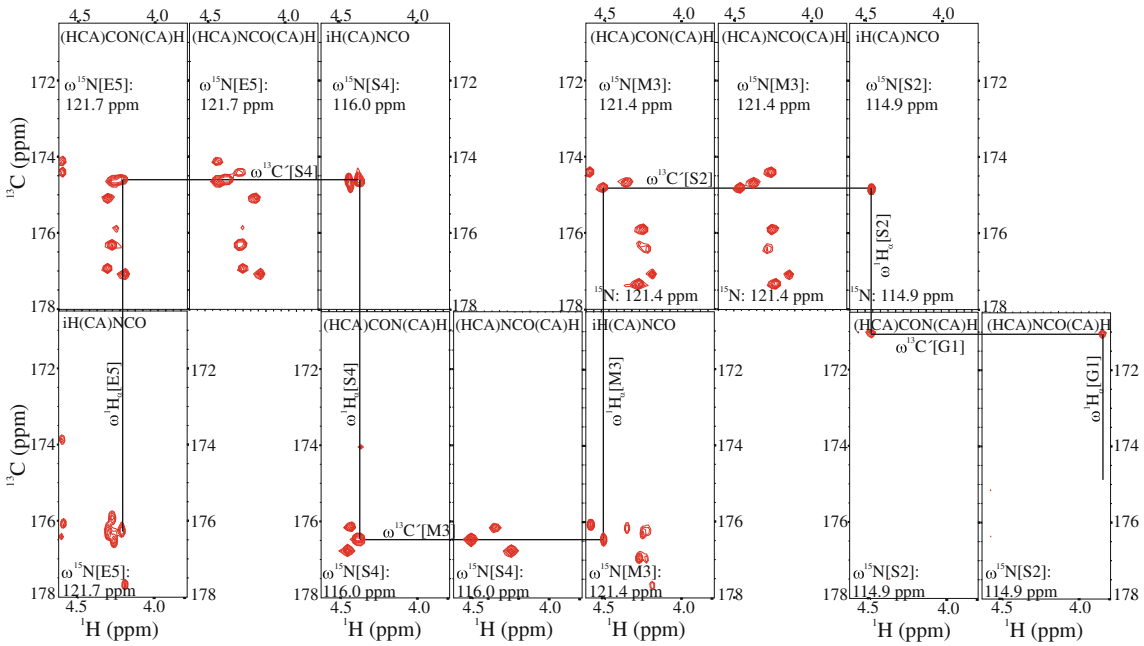

Fig. 6 Illustration of the 'sequential walk' by means of iH(CA)NCO, (HCA)CON(CA)H and (HCA)NCO(CA)H spectra. Strip plots showing $^{13}C'(i)$–$^{1}H(i)$, $^{13}C'(i-1)$–$^{1}H(i)$ and $^{13}C'(i-1)$–$^{1}H(i-1)$ projections of three-dimensional iH(CA)NCO, (HCA)CON(CA)H and (HCA)NCO(CA)H spectra taken at the chemical shift of $^{15}N(i)$ are shown. Assignment is exemplified using N-terminal residues G1–E5 of CT16, which remained unassigned from HN-detected experiments due to fast exchanging amide protons (Mäntylahti et al. 2009)

based assignment procedure due to exchange broadened amide proton resonances (Mäntylahti et al. 2009). The novel (HCA)CON(CA)H and (HCA)NCO(CA)H experiments utilize $^{13}C'$ spins for the sequential linking of consecutive residues, which perfectly coheres earlier approach based on ^{15}N chemical shift, thus minimizing ambiguous assignments due to degenerate ^{15}N chemical shifts. Moreover, unidirectional coherence transfer provides optimal spectral resolution by suppressing transfer routes, which would otherwise lead to unnecessary overlap with redundant information.

We reason that the assignment strategy based on HA-detection with unidirectional coherence transfer schemes will be very useful in case of intrinsically unfolded proteins and/or proteins that require relatively high pH (alkali) conditions.

Materials and methods

The novel (HCA)CON(CA)H and (HCA)NCO(CA)H schemes, and H(CA)NCO experiment were tested on 1.5 mM uniformly $^{15}N/^{13}C$ labeled immunoglobulin-binding domain B1 of streptococcal protein G (GB1, 6.5 kDa, 56 residues) dissolved in 20 mM potassium phosphate buffer, pH 5.5 with 7% D_2O in a 250 µl Shigemi micro-cell. In addition, iH(CA)NCO (Mäntylahti et al. 2010), (HCA)-CON(CA)H and (HCA)NCO(CA)H experiments were employed to the backbone assignment of 1 mM uniformly $^{15}N/^{13}C$ CT16 (110 residues) in 93/7% H_2O/D_2O by using two different buffers: 20 mM Sodium phosphate, 50 mM NaCl, pH 6.5 and 10 mM Tris–HCl, 50 mM NaCl, pH 8.5.

All the spectra were recorded at 25°C, on a Varian Unity INOVA 800 NMR spectrometer, equipped with a $^{15}N/^{13}C/^{1}H$ triple-resonance probehead and an actively shielded z-axis gradient system. For GB1, two-dimensional (HCA)CO(NCA)H ($T_{NC} = 15$ ms), (HCA)CO(NCA)H ($T_{NC} = 25$ ms) and H(CAN)CO spectra were measured (Fig. 4a–c). For each spectrum, 84 and 768 complex points in t_1 and t_2 were recorded using 8 transients per FID. This corresponds to acquisition times of 28 and 64 ms in t_1 ($^{13}C'$) and t_2 (^{1}H) dimensions. Total experimental time for each spectrum was 33 min. For CT16, three-dimensional (HCA)CON(CA)H ($T_{NC} = 25$ ms), HCA)NCO(CA)H ($T_{NC} = 25$ ms) and iH(CA)NCO experiments were measured at pH 6.5 and pH 8.5 using identical parameters: For (HCA)CON(CA)H and (HCA)NCO(CA)H experiments 86, 128 and 768 complex points in t_1 (^{13}C), t_2 (^{15}N), and t_3 (^{1}H), respectively, were collected. This translates into acquisition times of 33.1, 42.7 and 64 ms, respectively. For iH(CA)NCO, 128 (t_1, ^{15}N), 48 (t_2, ^{13}C) and 768 (t_3, ^{1}H) complex points were collected, yielding acquisition times of 42.7, 18.5 and 64 ms, respectively. For each experiment, two transients per FID were used. Total experimental time for (HCA)CON(CA)H and (HCA)NCO(CA)H experiments was 22 h each, and 16.5 h for iH(CA)NCO.

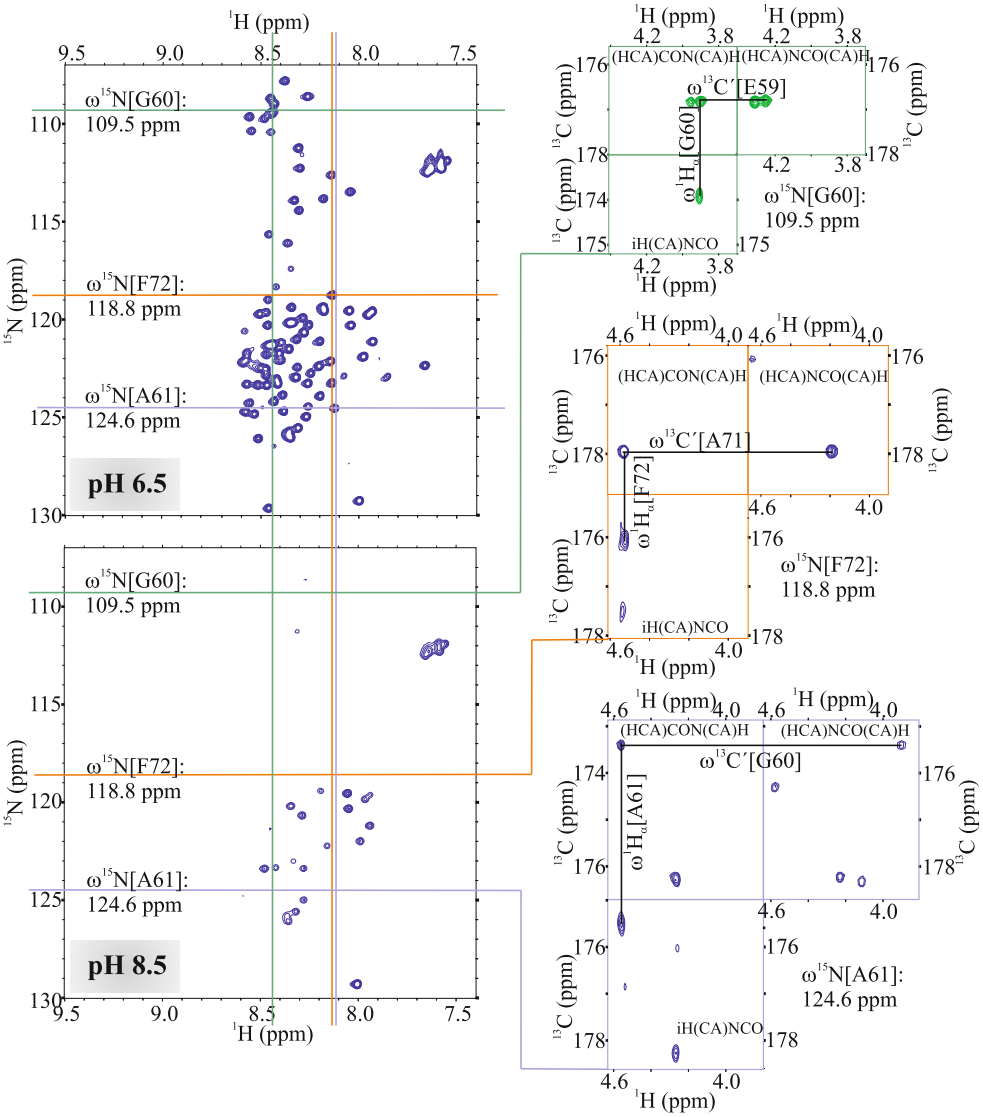

Fig. 7 iH(CA)NCO, (HCA)CON(CA)H and (HCA)NCO(CA)H spectra measured at high pH. Correlation peaks of example residues, G60, A61 and F72, are not visible in ^{1}H–^{15}N HSQC spectrum at pH 8.5 due to the enhanced chemical exchange at high pH. However, they are easily assignable from iH(CA)NCO, (HCA)CON(CA)H and (HCA)NCO(CA)H spectra as shown in plots of ^{13}C′(i)–^{1}H(i), ^{13}C′($i-1$)–^{1}H(i) and ^{13}C′($i-1$) –^{1}H($i-1$) projections at the chemical shift of ^{15}N(i). Crossing points of the color coded lines in both ^{1}H–^{15}N HSQC (at pH 6.5 and pH 8.5) spectra mark the position of potential HN cross peak and corresponding ^{15}N(i) planes of iH(CA)NCO, (HCA)CON(CA)H and (HCA)NCO(CA)H spectra are also shown. G60 is marked as green, A61 as violet and F72 as orange. Positive and negative peaks, appearing in the spectra, are marked as *blue* and *green*, respectively

Spectra were processed using the standard VNMRJ 2.2 revision D software package and analyzed with VNMRJ 2.2 revision D and Sparky 3.1.10 (Goddard and Kneller 2004). Prior to zero-filling to two-dimensional 4096 × 4096 data matrix (Fig. 4), or three-dimensional 512 × 512 × 2048 data matrix (Fig. 6) followed by the Fourier transform, the data were weighted with a shifted squared sine-bell functions applied to all three dimensions.

Acknowledgments This work was financially supported by the grants 122170 and 131144 (to P. P.) from the Academy of Finland. Sampo Mäntylahti acknowledges The National Doctoral programme in Informational and Structural Biology (ISB).

References

Alho N, Klaavuniemi T, Ylanne J, Permi P, Mattila S (2007) Backbone NMR assignment of the internal interaction site of ALP. Biomol NMR Assign 1:85–87

Bai Y, Milne JS, Mayne L, Englander SW (1993) Primary structure effects on peptide group hydrogen exchange. Proteins Struct Funct Genet 17:75–86

Bermel W, Bertini I, Felli IC, Piccioli M, Pierattelli R (2006) ^{13}C-detected protonless NMR spectroscopy of proteins in solution. Prog Nucl Magn Reson Spectr 48:25–45

Bermel W, Bertini I, Csizmok V, Felli IC, Pierattelli R, Tompa P (2009) H-start for exclusively heteronuclear NMR spectroscopy: the case of intrinsically disordered protein. J Magn Reson 198:275–281

Bottomley MJ, Macias MJ, Liu Z, Sattler M (1999) A novel NMR experiment for the sequential assignment of proline residues and proline stretches in ^{13}C/^{15}N-labeled proteins. J Biomol NMR 13:381–385

Bracken C, Palmer AG III, Cavanagh J (1997) (H)N(COCA)NH and HN(COCA)NH experiments for ^{1}H–^{15}N backbone assignments in ^{13}C/^{15}N-labeled proteins. J Biomol NMR 9:94–100

Delaglio F, Torchia DA, Bax A (1991) Measurement of ^{15}N–^{13}C J couplings in staphylococcal nuclease. J Biomol NMR 1:439–446

Dosztányi S, Csizmók V, Tompa P, Simon I (2005) IUPred: web server for the prediction of intrinsically unstructured regions of proteins based on estimated energy content. Bioinformatics 21:3433–3434

Dyson HJ, Wright PE (2001) Nuclear magnetic resonance methods for elucidation of structure and dynamics in disordered states. Methods Enzymol 339:258–270

Dyson HJ, Wright PE (2005) Intrinsically unstructured proteins and their functions. Nat Rev Mol Cell Biol 6:197–208

Fiorito F, Hiller S, Wider G, Wüthrich K (2006) Automated resonance assignment of proteins: 6D APSY-NMR. J Biomol NMR 35:27–37

Goddard T, Kneller D (2004) Sparky 3. University of California, San Francisco

Grzesiek S, Anglister J, Ren H, Bax A (1993) ^{13}C line narrowing by ^{2}H decoupling in ^{2}H/^{13}C/^{15}N-enriched proteins. Application to triple resonance 4D J connectivity of sequential amides. J Am Chem Soc 115:4369–4370

Grzesiek S, Bax A, Hu J-S, Kaufman J, Palmer I, Stahl SJ, Tjandra N, Wingfield PT (1997) Refined solution structure and backbone dynamics of HIV-1 Nef. Prot Sci 6:1248–1263

Hu K, Vögeli B, Clore GM (2007) Spin-state selective carbon-detected HNCO with TROSY optimization in all dimensions and double echo-antiecho sensitivity enhancement in both indirect dimensions. J Am Chem Soc 129:5484–5491

Kanelis V, Donaldson L, Muhandiram DR, Rotin D, Forman-Kay JD, Kay LE (2000) Sequential assignment of proline-rich regions in proteins: application to modular binding domain complexes. J Biomol NMR 16:253–259

Kay LE, Ikura M, Tschudin R, Bax A (1990) Three-dimensional triple-resonance NMR spectroscopy of isotopically enriched proteins. J Magn Reson 89:496–514

Kay LE, Keifer P, Saarinen T (1992) Pure absorption gradient enhanced heteronuclear single quantum correlation spectroscopy with improved sensitivity. J Am Chem Soc 114:10663–10665

Kupće E, Wagner G (1995) Wideband homonuclear decoupling in protein spectra. J Magn Reson 109A:329–333

Mäntylahti S, Tossavainen H, Hellman M, Permi P (2009) An intraresidual i(HCA)CO(CA)NH experiment for the assignment of main-chain resonances in ^{15}N, ^{13}C labeled proteins. J Biomol NMR 45:301–310

Mäntylahti S, Aitio O, Hellman M, Permi P (2010) HA-detected experiments for the backbone assignment of intrinsically disordered proteins. J Biomol NMR 47:171–181

Marion D, Ikura M, Tschudin R, Bax A (1989) Rapid recording of 2D NMR-spectra without phase cycling—application to the study of hydrogen-exchange in proteins. J Magn Reson 85:393–399

Marsh JA, Forman-Kay JD (2010) Sequence determinants of compaction in intrinsically disordered proteins. Biophys J 98: 2383–2390

Matsuo H, Kupce E, Li H, Wagner G (1996) Use of selective C^{α} pulses for improvement of HN(CA)CO-D and HN(COCA)NH-D experiments. J Magn Reson 111B:194–198

Morris GA, Freeman R (1979) Enhancement of nuclear magnetic resonance signals by polarization transfer. J Am Chem Soc 101: 760–762

Ogura K, Kumeta H, Inagaki F (2010) Structure determination of proteins in $^{2}H_2O$ solution aided by a deuterium-decoupled 3D HCA(N)CO experiment. J Biomol NMR 47:243–248

Panchal SC, Bhavesh NS, Hosur RV (2001) Improved 3D triple resonance experiments, HNN and HN(C)N, for HN and ^{15}N sequential correlations in (^{13}C, ^{15}N) labeled proteins: application to unfolded proteins. J Biomol NMR 20:135–147

Permi P (2002) Intraresidual HNCA: an experiment for correlating only intraresidual backbone resonances. J Biomol NMR 23: 201–209

Permi P, Annila A (2004) Coherence transfer in proteins. Prog Nucl Magn Reson Spectr 44:97–137

Pervushin K, Riek R, Wider G, Wüthrich K (1997) Attenuated T2 relaxation by mutual cancellation of dipole–dipole coupling and chemical shift anisotropy indicates an avenue to NMR structures of very large biological macromolecules in solution. Proc Natl Acad Sci USA 94:12366–12731

Rappu P, Nylund C, Ristiniemi N, Kulpakko J, Vihinen P, Hernberg M, Mirtti T, Alanen K, Kallajoki M, Vuoristo M-S, Pyrhönen S, Heino J (2010) Detection of melanoma-derived cancer–testis antigen CT16 in patient sera by a novel immunoassay. Int J Cancer. doi:10.1002/ijc.25571

Sattler M, Schleucher J, Griesinger C (1999) Heteronuclear multidimensional NMR experiments for the structure determination of proteins in solution employing pulsed field gradients. Prog Nucl Magn Reson Spectr 34:93–158

Schleucher J, Schwendinger MG, Sattler M, Schmidt P, Glaser SJ, Sørensen OW, Griesinger C (1994) A general enhancement scheme in heteronuclear multidimensional NMR employing pulsed-field gradients. J Biomol NMR 4:301–306

Shaka AJ (1985) Composite pulses for ultra-broadband spin inversion. Chem Phys Lett 120:201–205

Shaka AJ, Keeler J, Frenkiel T, Freeman R (1983) An improved sequence for broad-band decoupling—Waltz-16. J Magn Reson 52:335–338

Sun Z-YJ, Frueh DP, Selenko P, Hoch JC, Wagner G (2005) Fast assignment of ^{15}N-HSQC peaks using high-resolution 3D HNcocaNH experiments with non-uniform sampling. J Biomol NMR 33:43–50

Tossavainen H, Permi P (2004) Optimized pathway selection in intraresidual triple-resonance experiments. J Magn Reson 170: 244–251

Weisemann R, Rüterjans H, Bermel W (1993) 3D triple-resonance NMR techniques for the sequential assignment of NH and ^{15}N resonances in ^{15}N- and ^{13}C-labelled proteins. J Biomol NMR 3: 113–120

Yamazaki T, Lee W, Arrowsmith CH, Muhandiram DR, Kay LE (1994) A suite of triple-resonance NMR experiments for the backbone assignment of ^{15}N, ^{13}C, ^{2}H labeled proteins with high-sensitivity. J Am Chem Soc 116:11655–11666

Yamazaki T, Tochio H, Furui J, Aimoto S, Kyogoku Y (1997) Assignment of backbone resonances for larger proteins using the ^{13}C–^{1}H coherence of a $^{1}H_{\alpha}$-, ^{2}H-, ^{13}C-, and ^{15}N-labeled sample. J Am Chem Soc 119:872–880

Yao J, Dyson HJ, Wright PE (1997) Chemical shift dispersion and secondary structure prediction in unfolded and partly folded proteins. FEBS Lett 419:285–289